Title	Two-beam photoacoustic phase measurement of the thermal diffusivity of a Gd-doped bulk YBCO superconductor
Author(s)	Aravind, M; Fung, PCW; Tang, SY; Tam, HL
Citation	Review of Scientific Instruments, 1996, v. 67 n. 4, p. 1564-1569
Issued Date	1996
URL	http://hdl.handle.net/10722/42435
Rights	Creative Commons: Attribution 3.0 Hong Kong License

Two-beam photoacoustic phase measurement of the thermal diffusivity of a Gd-doped bulk YBCO superconductor

M. Aravind, P. C. W. Fung, S. Y. Tang, and H. L. Tam
Department of Physics, The University of Hong Kong, Hong Kong

(Received 8 May 1995; accepted for publication 4 January 1996)

The two-beam photoacoustic phase measurement was applied to measure quantitatively the thermal diffusivity (α_s) of a ceramic bulk high-T_c superconductor. Neglecting the effects of thermal dilation, and thermoelastic bending was proved valid in accordance with our composite piston model for the chosen experimental conditions. It was found that α_s shows different features at the onset and offset temperatures corresponding to the normal–superconducting (NS) transition. A dip was seen at the resistivity transition onset temperature and a cusp at the offset temperature where the electrical resistance disappears. The presence of the cusp at the offset temperature is proposed to be related to weak coupling between superconducting grains. Our studies indicate that the two-beam phase measurement is a very sensitive method for superconductor characterization and NS transition detection. The experimental results also confirm the presence of a large energy gap and strong electron–phonon coupling mechanism in the YBCO superconductor. © *1996 American Institute of Physics.* [S0034-6748(96)00504-0]

I. INTRODUCTION

Resistivity–temperature ($R-T$) and susceptibility–temperature ($\chi-T$) measurements, which probe the two basic aspects of superconductors—zero resistivity and perfect diamagnetism, respectively—are most common in superconductor characterization. However, in $R-T$ measurements if minority phases that are superconducting form paths in the sample, then an indication of zero resistance of the sample would lead us to the erroneous conclusion that the bulk is superconducting. Also, in $\chi-T$ measurements if a particle of the majority phase is shielded completely by a layer of superconducting minority phase on its surface then the transition of the latter might be mistakenly identified as being that of the whole particle volume.[1]

In view of the drawbacks in $R-T$ and $\chi-T$ measurements, various other methods have been adapted for superconductor characterization. Application of contactless methods, such as photoacoustic (PA)[2,3] and photothermal deflection (PTD) techniques,[4] has added a new dimension to normal–superconducting (NS) phase transition detection. They provide more direct, sensitive, economical, and convenient studies of the bulk features of any form of sample without special treatment. In this paper, we present our results on the thermal diffusivity measurement of a high-T_c superconductor ceramic sample using a two-beam photoacoustic phase measurement.[5] Advantages of our method over that of Song *et al.*,[2] who used a conventional single beam photoacoustic method, are elucidated in Sec. II. We have recorded the temperature dependence of thermal diffusivity of the sample and found different features corresponding to the NS transition onset and offset. These findings bear out the success of the PA method in superconductor characterization and NS transition detection.

II. TWO-BEAM PHOTOACOUSTIC PHASE MEASUREMENT

In the photoacoustic measurement of the diffusivity of solids,[6] the sample, with a backing material at its rear, is encased in a closed cell containing a gas and a sensitive microphone. The front surface of the sample is illuminated with a chopped monochromatic light beam. Light is absorbed by the sample periodically and is converted into thermal energy by a random deexcitation process. Thermal diffusion from the sample causes a periodic temperature variation in a thin layer of gas at the sample–gas boundary, which results in a pressure oscillation in the cell. This pressure oscillation, with the same period but not necessarily the same phase as the chopped light beam, induces an analog signal after it is picked up by the microphone. The phase difference is a consequence of the finite relaxation time in deexcitation. The expression for the pressure variation for an optically thick sample is well established:[7]

$$p_F=\frac{\gamma P_0 I_F}{2T_0 l_g K_s}\sqrt{\frac{\alpha_g}{\alpha_s}}\,\frac{g+\coth(l_s\sigma_s)}{I+g\,\coth(l_s\sigma_s)}\,\frac{1}{\sigma_s^2}, \tag{1}$$

where l is the thickness, α the thermal diffusivity, and K the thermal conductivity, with the subscripts g and s symbolizing that of the gas and the solid sample, respectively. T_0 and P_0 are the static temperature and pressure of the gas, respectively, and γ is the ratio of the heat capacities C_p/C_v of the gas. I_F stands for the power of light absorbed at the front surface. Similar effect could be detected in the case of rear-surface illumination and the pressure variation is expressible in the form[7]

$$p_R=\frac{\gamma P_0 I_R}{2T_0 l_g K_s}\sqrt{\frac{\alpha_g}{\alpha_s}}\,\frac{1}{\sinh(l_s\sigma_s)\left(1+\dfrac{g}{\tanh(l_s\sigma_s)}\right)}\,\frac{1}{\sigma_s^2}, \tag{2}$$

where the complex quantity is

$$\sigma_s=(1+i)\sqrt{\frac{\pi f}{\alpha_s}}, \tag{3}$$

and g is the ratio of thermal effusivities ($e=K/\alpha^{1/2}$) between the backing (e_b) and the sample (e_s), i.e.,

 0034-6748/96/67(4)/1564/6/$10.00

$$g=\frac{e_b}{e_s}=\frac{K_b}{K_s}\sqrt{\frac{\alpha_s}{\alpha_b}} \tag{4}$$

while f is the chopping frequency.

By visualizing Eqs. (1)–(4), we notice that if only one beam (either the front or the rear beam) is used, the signal depends on many parameters among which the power I_F (or I_R) of the absorbed light and the static pressure P_0 are difficult to measure. Although lots of parameters are eliminated by using signal magnitudes in both the front and the rear cases, namely,

$$\frac{|\delta p_F|}{|\delta p_R|}=\frac{I_F}{I_R}\sqrt{g^2(\cosh^2 x-\cos^2 x)+(\cosh^2 x-\sin^2 x)+g\ \sinh 2x}, \tag{5}$$

where

$$x=l_s\sqrt{\frac{\pi f}{\alpha_s}} \tag{6}$$

the powers of the absorbed light in the front and the rear surface are in general different. (This is due to the different surface conditions and the instability of the light source). However, I_F/I_R is still involved.

However, if the relative phases $\Delta\Psi=\Psi_F-\Psi_R$ of the signals from the front and the rear surfaces are measured, we can deduce x, hence α_s, regardless of the absorbed powers. Mathematical verification of this idea is presented below.

Phase angles of the photoacoustic signal relative to the chopped incident' light for the cases of front-surface illumination (Ψ'_F) and rear-surface illumination (Ψ'_R) can be deduced from Eqs. (1)–(4) as follows:

$$\tan\ \psi'_F=\frac{\sin^2 x(1+g\ \tanh x)(g+\tanh x)}{\tan x(1-g^2)\sin^2 x}, \tag{7a}$$

$$\tan\ \psi'_R=\frac{(g+\tanh x)}{\tan x(1+g\ \tanh x)}. \tag{7b}$$

In practice, an additional phase Ψ_0, which depends on the cell design and other experimental components being the same for the front and rear cases, is superimposed on both Ψ'_F and Ψ'_R,

$$\begin{aligned}\psi_F&=\psi'_F+\psi_0,\\ \psi_R&=\psi'_R+\psi_0\end{aligned} \tag{8}$$

but the relative phase is independent of Ψ_0:

$$\Delta\psi=\psi_F-\psi_R=(\psi'_F+\psi_0)-(\psi'_R+\psi_0)=\psi'_F-\psi'_R. \tag{9}$$

After simple algebrical steps we obtain

$$\tan(\Delta\psi)=\tan x\ \frac{g+\tanh x}{1+g\ \tanh x}. \tag{10}$$

It is clear that if $\Delta\Psi$ is measured and the value of g is known, x could be solved either graphically or numerically. The thermal diffusivity of the solid sample α_s can then be deduced from Eq. (6) from which the values of f and l_s could be easily measured. The merits of two-beam phase measurement over single-beam measurement are obvious: Owing to the independence of $\Delta\Psi$ on the power absorption of the sample surface, the two-beam phase measurement allows α_s of the sample to be measured directly. A further simplification of Eq. (10) can be done by using air backing. Since the effusivity of air is negligible compared to that of solid samples, we could set $g=0$ in Eq. (10) if the backing material used is air, and Eq. (10) simplifies to Pessoa's result:[5]

$$\tan(\Delta\psi)=\tan x\ \tanh x. \tag{11}$$

III. EFFECTS OF THERMAL DILATION AND THERMOELASTIC BENDING IN TWO-BEAM PHASE MEASUREMENT

Until now, we have been considering the contribution of the acoustic piston[6] (i.e., Rosencwaig and Gersho's consideration) to $\Delta\Psi$ only. Basically, two more mechanisms are involved. One of them is the thermal dilation effect,[7,8] which originates from the periodic expansion of the sample along its thickness after the sample was heated up by the chopped light beam. The significance of this effect depends on the mean sample temperature. Another effect one has to take into account is thermoelastic bending,[7,9] which is attributed to transverse thermal expansion and the existence of a nonzero temperature gradient throughout the thickness of the sample.

Rousset *et al.*[9] have derived the expression for the displacement of a point (r,z) in cylindrical coordinates in the sample from its equilibrium position due to heating of the sample by the light source in the case of rear illumination. Particularly in the z direction, the expression for the stated displacement is as follows:

$$u_z^R(r,z)=a_T\left\{\frac{6(R^2-r^2)}{l_s^3}M_T+\frac{1+\nu}{1-\nu}\int_{l_{s/2}}^{z}T_s^R dz-\frac{\nu}{1-\nu}\left[\frac{12M_T}{l_s^3}\left(z^2-\frac{l_s^2}{4}\right)+\frac{2N_T}{l_s}\left(z-\frac{l_s}{2}\right)\right]\right\} \tag{12}$$

with

$$M_T=\int_{-l_{s/2}}^{l_{s/2}}zT_s^R dz,\quad N_T=\int_{-l_{s/2}}^{l_{s/2}}T_s^R dz,$$

where a_T is the linear thermal expansion coefficient and ν is its Poisson ratio. The temperature distribution T_s^R inside a thermally thick sample is given by

$$T_s^R=\frac{I_0^R\cosh\left[\sigma_s\left(z-\frac{l_s}{2}\right)\right]}{2K_s\sigma_s\sinh(\sigma_s l_s)}. \tag{13}$$

By modifying Rousset's expression above to the case of front-surface illumination, we get

$$u_z^F(r,z)=a_T\left\{\frac{6(R^2-r^2)}{l_s^3}M_T+\frac{1+\nu}{1-\nu}\int_{l_s/2}^{z}T_s^F dz - \frac{\nu}{1-\nu}\left[\frac{12M_T}{l_s^3}\left(z^2-\frac{l_s^2}{4}\right)+\frac{2N_T}{l_s}\left(z+\frac{l_s}{2}\right)\right]\right\}, \tag{14}$$

where

$$T_s^F=\frac{I_0^F\cosh\left[\sigma_s\left(z+\frac{l_s}{2}\right)\right]}{2K_s\sigma_s\sinh(\sigma_s l_s)}. \tag{15}$$

In Eqs. (12) and (14) we noticed that only the first term is r dependent and represents the thermoelastic bending effect. The other terms are r independent and represent the effect of thermal dilation. So the thermoelastic bending effect is described by a quantity of the order of R^2/l_s^2 times larger than the thermal dilation effect, provided that the sample size satisfies $R>l_s$. Hence the second and latter terms in Eq. (14) can be neglected if $(R\gg l_s)$.

We can construct a composite piston as a sum of the acoustic piston (by RG) and thermoelastic bending

$$p_{F,R}=\delta p_{F,R}^{RG}+\delta p_{F,R}^{TB}, \tag{16}$$

where $\delta p_{F,R}^{RG}$ are given by Eqs. (1) and (2), respectively, and

$$\delta p_{F,R}^{TB}=\frac{\gamma P_0}{V_0}\int_0^R 2\pi r u_z^{F,R}\left(r,\frac{l_s}{2}\right)dr = (+,-)\,\frac{3}{2}\,\frac{\gamma P_0}{l_g}\,\frac{a_T I_0^{F,R}R^2}{K_s\sigma_s^3 l_s^3} \times\frac{\left(\frac{\sigma_s l_s}{2}\sinh(\sigma_s l_s)-\cosh(\sigma_s l_s)+1\right)}{\sinh(\sigma_s l_s)}. \tag{17}$$

By separating the real and imaginary parts in Eq. (17) and extracting the phase angles for both cases of front- and rear-surface illumination, we get

$$\tan\psi_F'=\frac{b(\cosh x-\cos x)[(\sinh x+\sin x)-x(\cosh x+\cos x)]-a\,\sinh x\,\cosh x}{b(\cosh x-\cos x)(\sinh x-\sin x)-a\,\sin x\,\cos x}, \tag{18a}$$

$$\tan\psi_R'=\frac{b(\cosh x-\cos x)[(\sinh x+\sin x)-x(\cosh x+\cos x)]+a\,\sinh x\,\cos x}{b(\cosh x\text{-}\cos x)(\sin x-\sinh x)+a\,\sin x\,\cosh x}, \tag{18b}$$

where

$$a=\frac{1}{T_0}\sqrt{\frac{\alpha_g}{\alpha_s}},\quad b=\frac{3a_T}{2x}\left(\frac{R}{l_s}\right)^2.$$

The relative phase has been found to be expressed by

$$\tan\Delta\psi=\frac{a\,\sin x\,\sinh x+b[x\,\sin x(\cos x+\cosh x)+\sinh^2 x-2\sin x\,\sinh x-\sin^2 x]}{a\,\cos x\,\cosh x+b[x\,\sinh x(\cos x-\cosh x)+\cosh^2 x-2\cos x\,\cosh x+\cos^2 x]} \tag{19}$$

in which terms containing b^2 in the denominator have been neglected. This assumption is valid for solids due to the small values of a_T (a_T is of the order of $10^{-5}\,\mathrm{K}^{-1}$ in solids). We observed from Eq. (19) that terms (in the denominator or associated numerator) with the coefficient "a" pertain to the acoustic piston effect while terms associated with the coefficient "b" arise from the effect of thermoelastic bending.

It is noteworthy that in Eq. (19), $\Delta\Psi$ is independent of the power absorbed by the sample. This property allows us to use a rather large power light source to increase the signal-to-noise ratio, without increasing the relative contribution of the thermoelastic bending effect to our measurement. This is the principal reason that prompted us to use two-beam PA phase measurement.

IV. VALIDITY OF ASSUMPTIONS

Before we proceeded to our measurements, we had to choose our chopping frequency f properly so that the assumptions for the equations in Sec. II would be valid.

First, justification of the assumption that the sample is optically thick is trivial, as it is optically opaque. Second, if

TABLE I. Effects of thermoelastic bending relative to the acoustic piston in two-beam photoacoustic phase measurement, $f=35$ Hz.

Temp (K)	α_s (cm^2/s)	a (K^{-1})	b (10^{-5} K^{-1})	b/a
	0.05	0.0190	20.47	0.011
	0.10	0.0130	28.95	0.022
293	0.50	0.0061	64.75	0.106
	1.00	0.0043	91.57	0.213
	0.05	0.0066	20.47	0.031
	0.10	0.0047	28.95	0.062
100	0.50	0.0021	64.75	0.309
	1.00	0.0015	91.57	0.610

the PA signal varies as f^q (where q is a constant) for $-1.5 \leqslant q < -1$ then the sample could be assumed to be thermally thick.[6] The stated condition is found to be so if the chopping frequency ranges from 5 to 50 Hz under our experimental conditions. Hence we chose 35 Hz as our chopping frequency. Finally, as the sample radius R is 8 times its physical thickness l_s, from Eqs. (12) and (14), the effect of thermoelastic bending is of the order of 64 times stronger than that of thermal dilation.

In view of Eqs. (19) and (6), as the parameter b depends on the choice of f, we have compared the relative contribution from the acoustic piston and thermoelastic bending to $\Delta\Psi$ by calculating the ratio b/a at $f=35$ Hz at 293 K (room temperature) and 100 K, respectively, for several values of α_s ranging from 0.05 to 1 $cm^2\ s^{-1}$. The results are tabulated in Table I. The effect of the acoustic piston is shown to always be dominating especially when α_s is small. For $\alpha_s < 0.5$, we can neglect the effect of thermoelastic bending on $\Delta\Psi$, as the acoustic piston effect is two orders of magnitude larger than the thermoelastic bending effect. Then we can simply apply Eq. (11) instead of Eq. (19) for calculating α_s.

To check the validity of our theoretical model we have used the same method to determine the thermal diffusivity of various metals—whole thermal diffusivity values are known. The result of this analysis is shown below in Table II.[21]

From Table II it can be seen that the experimental values agree quite well with the literature values and hence confirm the validity of the theoretical model we have used. In calculating the value of α for the metals, the thermoelastic effect was also taken into account in addition to the thermal diffusion effect.

Though the thermal expansion coefficient of metals and the superconductors are roughly the same, the effect of thermoelastic bending is neglected in the case of the YBCO sample under our experimental conditions. This is justified as can be seen from the large value of a in Table I as compared to the value of b.

TABLE II. The thermal diffusivity values obtained for different metals using our theoretical model.

Sample	Thickness l (mm)	Measured α (cm^2/s)	Literature value α (cm^2/s)
Aluminum	0.55	0.82	0.84[a]
Copper	1.00	1.13	1.12[a]
Iron	0.50	0.22	0.20[a]
Lead	0.50	0.21	0.23[a]
Silicon	0.52	0.72	0.76[b]

[a]Reference 21.
[b]Reference 22.

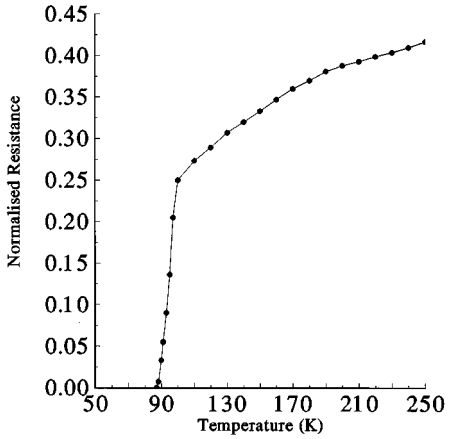

FIG. 1. Normalized $R-T$ curve of our $Y_{0.6}Gd_{0.4}Ba_2Cu_3O_7$ sample. The resistance has been normalized to the value at room temperature.

V. EXPERIMENTATION

The bulk sample used was polycrystalline Gd-doped YBCO[11,12] with a nominal composition of $Y_{0.6}Gd_{0.4}Ba_2Cu_3O_7$, which was fabricated by simple solid state reaction. AR grade Y_2O_3, Gd_2O_3, BaO, and CuO powders were mixed in the required ratio and ground thoroughly to a homogeneous mixture, which was preheated to 954 °C for 24 h. Grinding and preheating were repeated again to promote homogeneity before the powder was pelletized and sintered at 964 °C for 24 h in flowing oxygen. Annealing was then performed at 300 °C for another 20 h in an oxygen-rich atmosphere.

The normalized resistance–temperature graph of the sample is shown in Fig. 1. The resistance values are normalized to the value of the resistance at room temperature, which is nearly 10^{-1} Ω. The measurement was taken in decreasing temperature. The transition onset was found to occur at 100 K while the offset at 88 K.

The two-beam PA phase detection was performed in the following manner. The experimental setup is schematically depicted in Fig. 2. A Coherent–Innova 70, argon-ion laser (wavelength of 5145 Å, output power of 6W) was used as the light source. Periodic heating of the sample was achieved by chopping the laser beam, using a Stanford SR 540 mechanical chopper. The chopping frequency was chosen to be 35 Hz, so that the assumptions for the equations in Sec. II are valid. The sample, in the form of a circular disc of radius (R) 4 mm and thickness (l_s) 0.5 mm was rigidly clamped on the sample chamber of a homemade PA cell such that the front surface of the sample is inside the chamber while the rear surface is opened to the bottom of the cryostat. The PA cell is of the Helmholtz resonator type[13,14] with a resonant frequency of 484 Hz at room conditions. So, measurements were performed in nonresonant mode (as $f=35$ Hz). The PA cell was filled with dry nitrogen gas at a pressure of 0.58 bar. No special backing material was used. Cooling was achieved

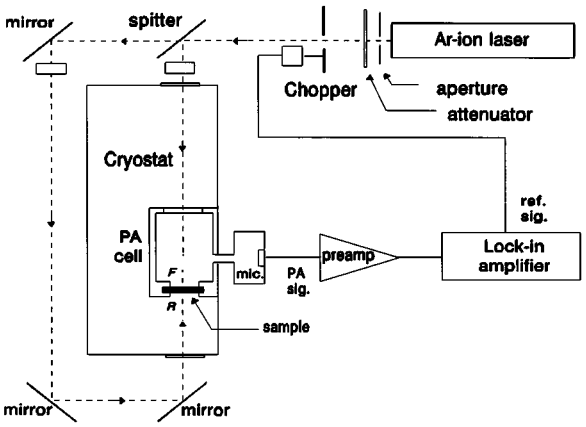

FIG. 2. Schematic diagram showing the experimental setup for two-beam photoacoustic phase measurement of thermal diffusivity.

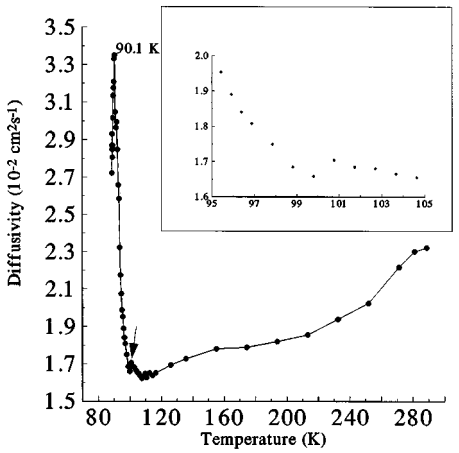

FIG. 3. $\alpha_s - T$ curve of our $Y_{0.6}Gd_{0.4}Ba_2Cu_3O_7$ sample. The insert shows the curve in expanded scale in temperature near transition onset.

by placing the PA cell inside a liquid nitrogen cryostat, which was equipped with a heater for temperature variation. The temperature was varied from room temperature down to 77 K and the value was measured by a calibrated platinum resistance thermometer with a resolution of 0.1 K. The PA signal in the form of pressure variation was detected by an Electret microphone capsule KE 4-211-1 inside the microphone chamber, which was connected to the sample chamber by a capillary. The acoustic signal from the microphone was preamplified. The phase of this signal was compared with that of the reference signal from the chopper by a Stanford SR 530 phase lock-in amplifier. Due to apparatus limitation, front and rear illuminations were performed separately. Rear-surface measurement was performed using the mirror under the PA cell as shown in Fig. 2. All measurements were performed on a Newport RS4000 optical table to minimize spurious signals due to unwanted vibration.

VI. RESULTS AND ANALYSIS

The sample was cooled in zero-magnetic field from 300 down to 87 K. Measurement was performed for each degree decrease of temperature near the expected transition range. Ψ_F and Ψ_R were measured directly by the lock-in amplifier. $\Delta\Psi$ at various temperatures were obtained simply by subtracting Ψ_R from Ψ_F. The values of $\Delta\Psi$ were fed into Eq. (11) and x was solved. Thermal diffusivity of the sample α_s can be deduced easily from Eq. (6). The $\alpha_s - T$ plot is shown in Fig. 3.

We first noticed that α_s is of the order of magnitude 0.01 $\mathrm{cm^2\,s^{-1}}$. From Table I the ratio b/a is smaller than 0.01, which confirms the validity of applying Eq. (11) instead of Eq. (19), i.e., neglecting the effect of thermoelastic bending. Second, α_s showed a sharp cusp in the vicinity of 90 K.

By comparing the $\alpha_s - T$ curve to the $R - T$ curve, we find that the cusp with a falling edge at 90 K in the $\alpha_s - T$ curve corresponds exactly to the resistive transition offset and the minor dip found at 100 K in the $\alpha_s - T$ curve correlates very well with the resistive transition onset. The falling edge in the cusp was predicted but not observed by Issac *et al.*,[15] who adopted single-beam PA measurement on $YBa_2Cu_3O_7$. The result was seen by Peralta *et al.*,[23] who used photopyroelectric impulse response methods on similar samples.

We believe that the minor dip in α_s at the resistivity transition onset temperature is a result of the abrupt increase in the electron specific heat[16,17] (due to the onset of superconductivity in individual grains). This can be visualized from the definition of thermal diffusivity viz. $\alpha_s = K_s/\rho_s C_p$ in which C_p is the total (electrons and lattice) isobaric heat capacity.

Besides we find that the increase in α below T_c must be due to the increase in the mean-free path of phonons.[18] Below T_c the charge carriers condense to form Cooper pairs which do not scatter phonons, and as a result the mean-free path of phonons will increase. It is seen that below T_c, for high temperature YBCO samples, the thermal conductivity increases gradually[18] though the specific heat decreases rapidly[19] with decreasing temperature. These two effects cause the increase in the thermal diffusivity below T_c to be very sharp. The sharp increase in the thermal diffusivity marks the onset of superconductivity. There is a competition between the rapidly diminishing electronic component of heat transport and the increasing phononic component. The cusp in the $\alpha_s - T$ curve is a result of this competition and coincides very well with the resistive transition offset temperature.

The increase in the thermal diffusivity is seen to be very steep and this may be due to the presence of a large energy gap in the superconductor. When the gap is larger the electrons condense more rapidly with decreasing temperature and the scattering of phonons by electrons will decrease. The cusp is seen at not too low a temperature as compared to the transition onset temperature, this predicts a strong electron–phonon coupling. The cusp shifts to a temperature nearer the transition temperature for a coupling strength greater than the BCS one.[20] The falling edge of the cusp is due to the decrease of the phonon population at very low temperatures and is also due to phonon scattering. Our sample is polycrystalline and hence superconducting grains may be present which can form tunneling states. These states form the phonon scattering entities at low temperatures and hence the decrease in thermal diffusivity. The presence of the cusp in-

dicates the importance of phonon–carrier interaction in the normal state of the Gd-doped YBCO samples. This effect is difficult to observe in conventional superconductors because of their large carrier concentration. We see that the cusp is the effect of the granular nature of the polycrystalline superconductor.

Due to the short coherence length ξ of cuprate superconductors [for $YBa_2Cu_3O_7$,[19] $\xi_{ab}(0)=34$ Å, $\xi_c(0)=7$ Å], weak-link behavior was expected near T_c. Superconducting grains (here the term ''grains'' does not just imply physical grains but also superconducting portions separated by twin boundaries within physical grains) in polycrystalline samples start to couple weakly with their neighbors at T_c. At $T^*<T_c$ (Ref. 18) all the grains are coupled together and bulk superconductivity starts to occur. Once coupling between superconducting grains starts, the Gibb's free energy of the system must also include the coupling energy between grains. The inclusion of the coupling energy in the Gibb's free energy implies abrupt changes in the heat capacity, which varies as the second derivative of the total Gibb's free energy with respect to temperature. Such behavior was revealed by the cusp in the α_s-T curve at T^*, which coincides with the resistive transition offset temperature.

ACKNOWLEDGMENTS

This work was supported by the Research Grant Council of Hong Kong and a University of Hong Kong Post-Graduate Student Grant.

[1] V. Z. Kresin and S. A. Wolf, *Fundamentals of Superconductivity* (Plenum, New York, 1990).
[2] Y. S. Song, H. K. Lee, and N. S. Chung, J. Appl. Phys. **65**, 2568 (1989).
[3] Y. S. Song and N. S. Chung, J. Appl. Phys. **67**, 935 (1990).
[4] K. C. Tsui, P. C. W. Fung, H. L. Tam, and G. O. Walker, J. Phys. Chem. Solids **52**, 979 (1991).
[5] O. Pessoa, Jr., C. L. Cesar, N. A. Patel, H. Vargas, C. C. Ghizoni, and L. C. M. Miranda, J. Appl. Phys. **59**, 1316 (1986).
[6] A. Rosencwaig and A. Gersho, J. Appl. Phys. **47**, 64 (1975).
[7] P. Charpentier, F. Lepoutre, and L. Bertrand, J. Appl. Phys. **53**, 608 (1982).
[8] F. A. McDonald and G. C. Wetsel, Jr., J. Appl. Phys. **49**, 2313 (1978).
[9] G. Rousset, F. Lepoutre, and L. Bertrand, J. Appl. Phys. **54**, 2383 (1983).
[10] L. K. T. Christopher, *Photoacoustic Studies of Condensed Matter* (unpublished).
[11] Z. Qi-Rui, Q. Yi-Tai, and C. Zu-Yao, Solid State Commun. **63**, 415 (1987).
[12] H. G. A. Yuzhen, C. Genhua, and C. Liquan, Int. J. Mod. Phys. B **1**, 199 (1987).
[13] G. A. West, J. J. Barrett, D. R. Siebert, and K. Virupaksha Reddy, Rev. Sci. Instrum. **54**, 797 (1983).
[14] Fernelius, Appl. Opt. **18**, 1784 (1979).
[15] J. Isaac, J. Philip, and B. K. Chaudhuri, Pramana Ind. J. Phys. **32**, L167 (1989).
[16] M. Tinkham, *Introduction to Superconductivity* (McGraw-Hill, New York, 1975).
[17] N. E. Phillips, J. E. Emerson, and R. A. Fisher, J. Superconduct. **7**, 251 (1994).
[18] C. E. Gough, IBM J. Res. Dev. **33**, 262 (1989).
[19] T. K. Worthington, W. J. Gallagher, and T. R. Dinger, Phys. Rev. Lett. **59**, 1160 (1987).
[20] L. Tewordt and Th. Wolkhausen, Solid State Commun. **70**, 839 (1989).
[21] E. Eckert and R. Drake, Jr., *Analysis of Heat and Mass Transfer* (McGraw-Hill, Kogakusha, 1972).
[22] *CRC Handbook of Chemistry and Physics*, 72nd ed. (Chemical Rubber, Boca Raton, FL, 1991/92).
[23] S. B. Peralta, I. A. Vitkin, K. Ghandi, A. Mandelis, W. Sadowski, and E. Walker, in *Photoacoustic and Photothermal Phenomena II*, edited by J. C. Murphy (Springer, Berlin, 1990).